Available online at www.sciencedirect.com
SCIENCE DIRECT®
Scripta Materialia 53 (2005) 1455–1460
Scripta MATERIALIA
www.actamat-journals.com

Using friction stir processing to fabricate MgAlZn intermetallic alloys

C.H. Chuang, J.C. Huang *, P.J. Hsieh

Institute of Materials Science and Engineering, Center for Nanoscience and Nanotechnology, National Sun Yat-Sen University, Kaohsiung 804, Taiwan, ROC

Received 6 July 2005; received in revised form 1 August 2005; accepted 9 August 2005
Available online 22 September 2005

Abstract

Friction stir processing (FSP) is applied in mixing elemental thin sheets of Mg, Al, and Zn in various portions, resulting in hard intermetallic alloys with Vicker's hardness in excess of 350. The $Mg_3Al_2Zn_3$ τ phase formed at ~360 °C during FSP, coupled with some other binary or ternary phases of nano size, accounts for the high hardness.

Keywords: Friction stir processing; Intermetallic alloys; Hardness; Magnesium alloy

1. Introduction

The friction stir welding technique, developed by The Welding Institute (TWI) in the United Kingdom [1], is a potentially attractive joining technique and has been extensively applied in aluminum alloys. Later modifications by Mishra et al. [2,3] to develop friction stir processing (FSP) have also attracted attention. FSP has been demonstrated to be an effective means of refining the grain size of cast or wrought aluminum or magnesium based alloys via dynamic recrystallization [4–8]. Moreover, the severe plastic deformation and material flow in the stirred zone can be utilized to achieve surface or bulk alloy modification via mixing of other elements or second phases into the stirred alloys. As a result, the stirred material can become a metal matrix composite [9–11] or an intermetallic alloy with much higher hardness and wear resistance.

In this paper, the feasibility of fabricating multi-elemental Mg–Al–Zn intermetallic alloys is demonstrated. Commercial cast or wrought type Mg–Al–Zn AZ-series alloys, such as AZ91, AZ61 or AZ31 with 3–9 wt.% Al and 1 wt.% Zn, have been widely used in automobiles or electronic appliances. The hardness of the AZ-series alloys is typically in the range of 50–100 H_v, and they suffer from insufficient creep resistance. Many academic and industrial research teams have made great efforts to improve the strength, hardness and creep properties of the commercial magnesium alloys by adding rare earth elements or ceramic reinforcements. In the current study, an alternative approach is used by mixing a much higher portion (10–30 wt.%) of the existing solute elements Al and Zn through FSP.

2. Experimental methods

The base Mg chosen was the more deformable AZ31 commercial Mg alloy, purchased from the CDN Company, Delta, BC, Canada, with the chemical composition of Mg–3.02 wt.%Al–1.01 wt.%Zn. The as-received AZ31 alloy was fabricated through semi-continuous casting and has the form of an extruded billet measuring 178 mm in diameter and 300 mm in length, with nearly equiaxed grains around 75 μm (all grain sizes hereafter were measured based on the linear line intercept method). The AZ31 billet was then warm rolled to 1 mm in thickness. Pure Al and pure Zn foils of 99.9% purity and 0.2 and 0.125 mm in thickness, respectively, were adopted for mixing with the AZ31 sheets. With the desired portions of Mg, Al, and Zn, the thin foil specimens were stacked as a sandwich and held vertically as shown in Fig. 1, ready for FSP.

* Corresponding author. Tel.: +886 7 525 2000x4063; fax +886 7 525 4099.
E-mail address: jacobc@mail.nsysu.edu.tw (J.C. Huang).

1359-6462/$ - see front matter © 2005 Acta Materialia Inc. Published by Elsevier Ltd. All rights reserved.
doi:10.1016/j.scriptamat.2005.08.019

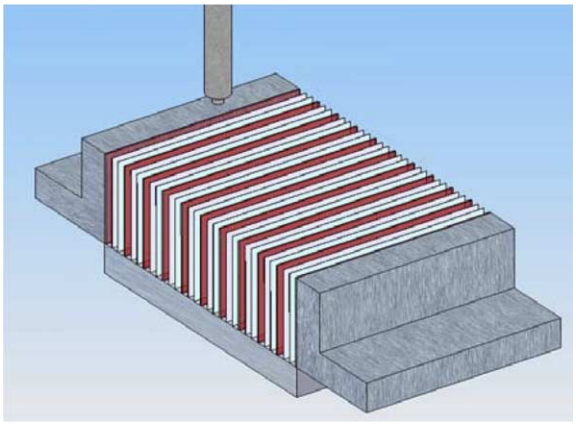

Fig. 1. Schematic illustration of the stacked AZ31 Mg alloy sheets (1 mm thick in dark contrast) with pure Al and pure Zn foils (0.2 mm and 0.125 mm thick in lighter contrast).

The simplified FSP machine was a modified form of a horizontal-type miller, with a 5 HP capability. The fixed pin tool was 6 mm in diameter and 5 mm in length, with a pitch distance of 1.2 mm. The shoulder diameter was 16 mm, and the tilt angle of the fixed pin tool was 2°. The pin rotation was set to be 1500 rpm, and the pin advancing speed was 20 mm/min. Selected FSP runs were conducted using liquid N_2 to chill the specimens and the rotating pin. A special container was placed around the specimen so that the specimen and pin could be submerged in the liquid N_2, as shown in Fig. 2. Two K type thermocouples were inserted into the specimen to monitor the temperature history during FSP. It was found that the maximum temperature rises in specimens without and with liquid N_2 were around 550 °C and 450 °C, respectively. Both are higher than the melting temperature of Zn, namely, 420 °C. The time duration for the temperature rise at any location without liquid N_2 cooling was typically 450 s, approximately 150 s for the temperature to rise and 300 s to cool down. With liquid N_2 cooling, the temperature rise time duration became shorter, being around 100 s for the temperature to rise and 150 s to cool down.

The processed specimens are examined by optical, scanning or transmission electron microscopy (OM, SEM, or TEM), and were characterized by X-ray diffraction (XRD) and Vicker's microhardness (H_v) measurements.

3. Results and discussion

3.1. Microstructure

The stir zone for the multi-element intermetallic specimen was typically about the size of the rotating pin, namely 6 mm in width and 5 mm in depth, which is smaller than the dynamically recrystallized zone seen in the AZ31 Mg alloys (~9 mm in width and 6 mm in depth) [8]. It is conceivable that the intermetallic specimens are much harder and become less deformable during FSP.

The original trial started from the $Mg_{80}Al_{10}Zn_{10}$ system without adding liquid N_2 cooling. After two or three passes of FSP, the microstructure, observed by SEM back scattering imaging (BEI), contains a fine grained darker Mg (measuring 0.2–2 μm) surrounded by lighter Al and nearly white Zn, as shown in Fig. 3. The low melting Zn ($T_m \sim 420$ °C) appears to have fully melted during FSP and is squeezed into a thin layer coating the Mg grains. There are a few large particles with distinct contrast in Fig. 3. These particles are typically around 5 μm in size, and the composition determined by SEM energy dispersive spectrometry (EDS) is close to $Mg_3Al_2Zn_3$ (sometimes defined as the $Mg_{32}(Al,Zn)_{49}$) τ phase, with a cI162 space group and a cubic lattice constant of 1.42 Å.

For higher Al and Zn content, to compositions of $Mg_{70}Al_{15}Zn_{15}$ and $Mg_{60}Al_{20}Zn_{20}$, the τ phase emerged even earlier after the first pass of FSP. With further FSP passes, the τ particles gradually became the dominant phase, as shown in Fig. 4. The volume fractions of the τ phase in the above three systems are listed in Table 1.

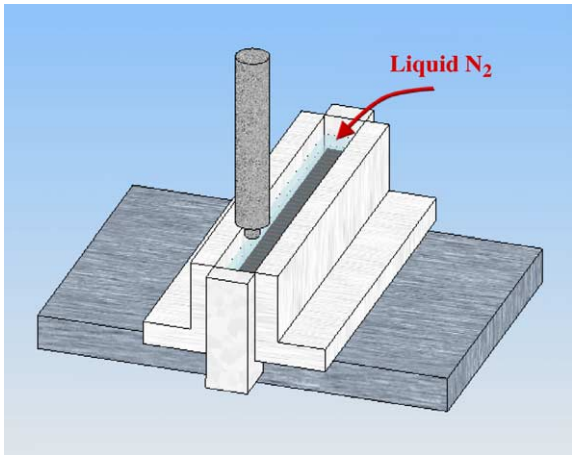

Fig. 2. Schematic illustration of the fixture used for liquid N_2 cooling.

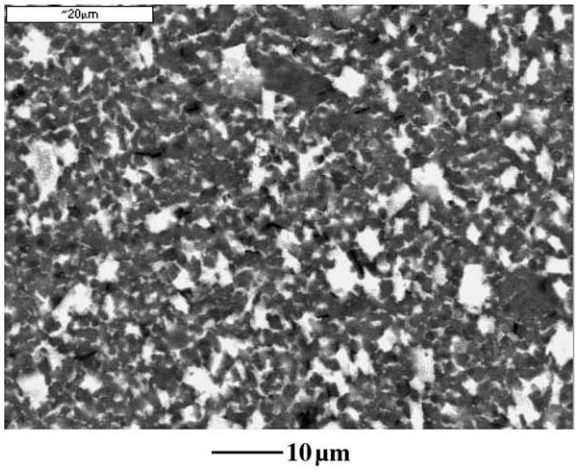

Fig. 3. SEM/BEI micrographs showing the phase dispersion in the $Mg_{80}Al_{10}Zn_{10}$ system after three passes. The white contrast Zn appears to have melted and coats the Mg/Al phases.

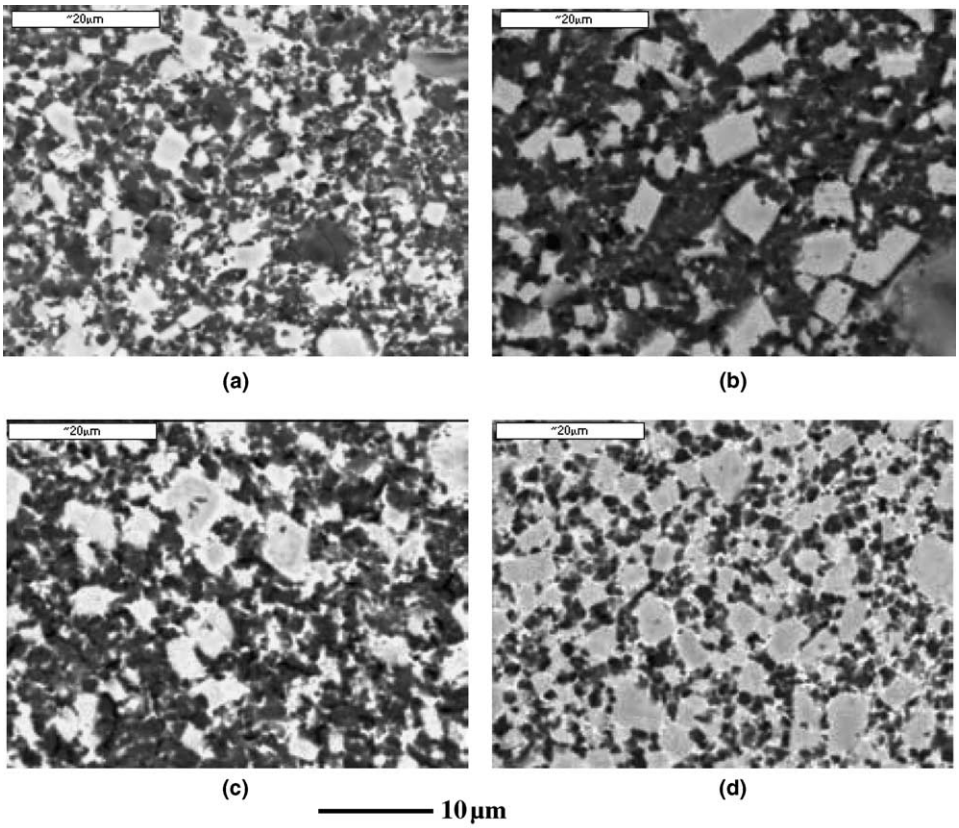

Fig. 4. SEM/BEI micrographs of the $Mg_{70}Al_{15}Zn_{15}$ system after two and three passes (a) and (b), and the $Mg_{60}Al_{20}Zn_{20}$ system after two and three passes (c) and (d).

Table 1
Summary of the volume fraction of the τ phase and H_v microhardness in the FSP processed intermetallic alloys after three passes with or without liquid N_2 cooling

Alloy system	Cooling	Vol.%	Average H_v
AZ31	No liq N_2	0	60
$Mg_{80}Al_{10}Zn_{10}$	No Liq N_2	29.4	133 ± 8
$Mg_{70}Al_{15}Zn_{15}$	No Liq N_2	41.7	187 ± 24
$Mg_{60}Al_{20}Zn_{20}$	No Liq N_2	65.4	216 ± 16
$Mg_{80}Al_{10}Zn_{10}$	With Liq N_2	–	–
$Mg_{70}Al_{15}Zn_{15}$	With Liq N_2	40.1	216 ± 23
$Mg_{60}Al_{20}Zn_{20}$	With Liq N_2	63.6	244 ± 7
$Mg_{60}Al_{15}Zn_{25}$	No Liq N_2	66.0	227 ± 10
$Mg_{50}Al_{20}Zn_{30}$	No Liq N_2	69.8	240 ± 18
$Mg_{37.5}Al_{25}Zn_{37.5}$	No Liq N_2	82.1	330 ± 47

With the cooling rate improved by adding liquid N_2, the microstructures tend to be more uniformly distributed and even smaller τ particles are induced, as shown in Fig. 5. The volume fractions of the τ phase in specimens with or without liquid N_2 cooling are close, as shown in Table 1.

Systematic SEM/EDS measurements for the white contrast phase have been conducted. It is consistently found that the composition of this phase is close to $Mg_{49.2\pm1.8}Al_{17.2\pm1.5}Zn_{33.6\pm1.8}$, not far from the $Mg_3Al_2Zn_3$ τ phase, as determined by XRD and TEM. Therefore, alternate alloy systems are prepared for FSP, namely, the $Mg_{60}Al_{15}Zn_{25}$, $Mg_{50}Al_{20}Zn_{30}$, and $Mg_{37.5}Al_{25}Zn_{37.5}$ systems. The typical SEM/BEI micrograph is shown in Fig. 6. The τ volume fraction can be further increased, as detailed in Table 1.

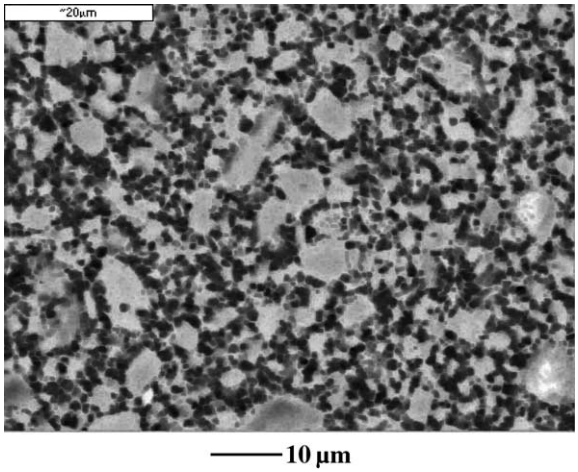

Fig. 5. SEM/BEI micrographs showing the phase dispersion in the $Mg_{60}Al_{20}Zn_{20}$ system after three passes with liquid N_2 cooling.

3.2. X-ray diffraction

When the Al and Zn contents were low (10 at.% each), the XRD patterns of the $Mg_{80}Al_{10}Zn_{10}$ system resembled

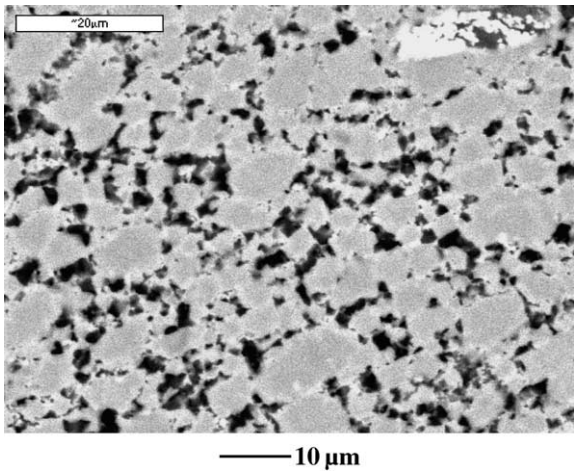

Fig. 6. SEM/BEI micrograph showing the phase dispersion in the $Mg_{37.5}Al_{25}Zn_{37.5}$ system after three passes without liquid N_2 cooling.

those of the FSP AZ31 alloys, with the three most notable peaks of $(10\bar{1}0)$, (0002) and $(10\bar{1}1)$, as seen in Fig. 7(a). The diffraction peaks gradually declined and broadened with increasing FSP passes, suggesting the overall refinement of the microstructure. With much more Al and Zn in $Mg_{60}Al_{20}Zn_{20}$, the XRD pattern in Fig. 7(b) is replaced by multiple phases, including the intermediate phases of $Mg_3Al_2Zn_3$, Mg_2AlZn and Mg_4AlZn_{11}, and possibly some others. The peak broadening becomes more apparent in $Mg_{50}Al_{20}Zn_{30}$ or $Mg_{37.5}Al_{25}Zn_{37.5}$, as shown in Fig. 8. It appears that the increasing FSP passes, higher Al and Zn contents, and accelerating cooling rate by liquid N_2 are promising means of refining grains to submicron- or nano-scales.

A slight hump in the XRD curves within $2\theta = 25$–$33°$ (centering at $2\theta \sim 30°$) can be seen, especially for specimens with higher Al and Zn contents or when liquid N_2 cooling is used, suggesting that a partial amorphous phase has been induced. The *d*-spacing values corresponding to such Bragg angles are 2.71–3.56 Å, centering at 2.98 Å. Since the atomic radii of Mg, Al, and Zn are 1.60, 1.43, and 1.35 Å, the average atom spacing in a completely amorphous alloy with nominal compositions around $Mg_{60}Al_{20}Zn_{20}$ and $Mg_{37.5}Al_{25}Zn_{37.5}$ would be around 2.93 and 3.03 Å, respectively, very close to the observed average 2.98 Å. It is conceivable that the very small amount of the amorphous phase would have the composition close to $Mg_3Al_2Zn_3$,

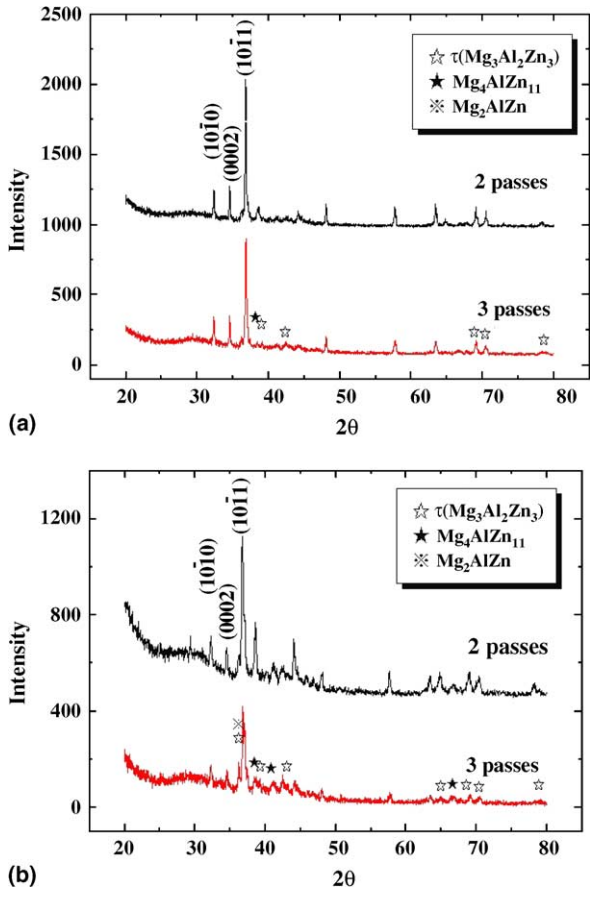

Fig. 7. The XRD patterns for (a) $Mg_{80}Al_{10}Zn_{10}$ and (b) $Mg_{60}Al_{20}Zn_{20}$ systems.

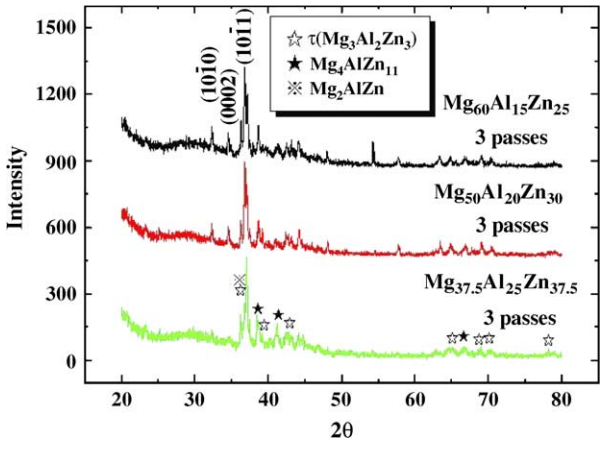

Fig. 8. The analysis of XRD for $Mg_{60}Al_{15}Zn_{25}$, $Mg_{50}Al_{20}Zn_{30}$, and $Mg_{37.5}Al_{25}$ $Zn_{37.5}$ after three passes without liquid N_2 cooling.

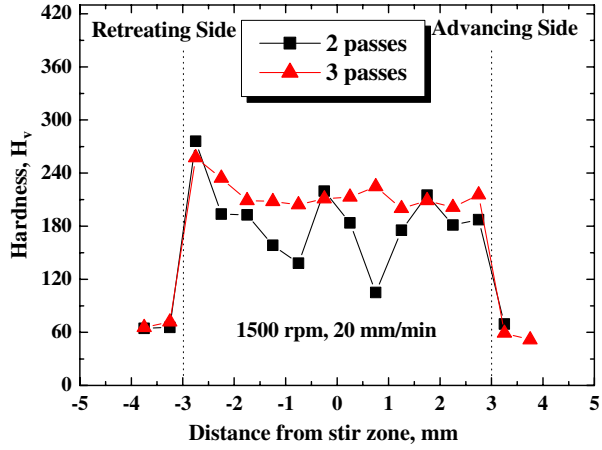

Fig. 9. The variation of H_v along the transverse cross-sectional plane of the $Mg_{60}Al_{20}Zn_{20}$ system.

which is also a phase formed at the low melting eutectic point (~362 °C). It is consistent with the general observation that an amorphous phase tends to form at the eutectic composition [12].

3.3. Hardness measurement

The typical hardness measurement results along the transverse cross-sectional plane are depicted in Fig. 9. Increasing the FSP passes would raise the H_v values and reduce the variation of H_v readings inside the nugget zone, or the system contains more intermetallic phases and the microstructure becomes more uniform. Meanwhile, the hardness is seen to gradually increase with increasing Al and Zn contents. With liquid N_2 cooling, the hardness is slightly higher than the same alloy system without liquid N_2 (Fig. 10). The maximum hardness approaches nearly 400 H_v in the $Mg_{37.5}Al_{25}Zn_{37.5}$ system after three passes without the liquid N_2 cooling, as shown in Fig. 11. The average H_v values in the various alloy systems are also compared in Table 1. A direct relationship between H_v and τ volume fraction is seen.

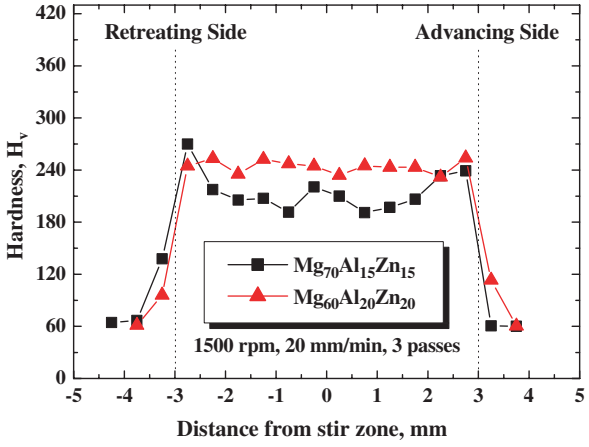

Fig. 10. The variation of H_v along the transverse cross-sectional plane of $Mg_{70}Al_{15}Zn_{15}$ and $Mg_{60}Al_{20}Zn_{20}$ after three passes with liquid N_2 cooling.

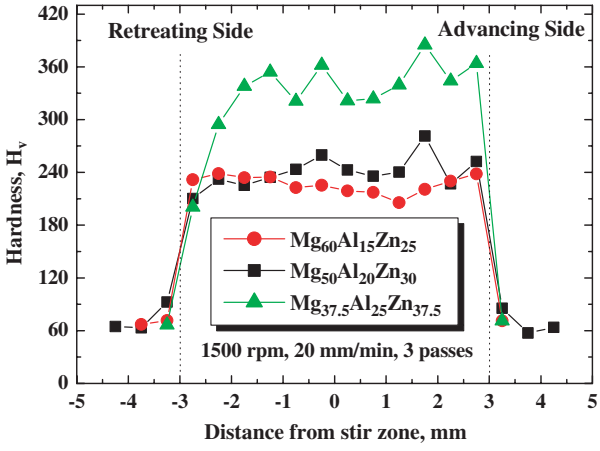

Fig. 11. The variation of H_v along the transverse cross-sectional plane of $Mg_{60}Al_{15}Zn_{25}$, $Mg_{50}Al_{20}Zn_{30}$, and $Mg_{37.5}Al_{25}$ $Zn_{37.5}$ after three passes without liquid N_2 cooling.

3.4. TEM examination

Systematic TEM characterization of the $Mg_{50}Al_{20}Zn_{30}$ and $Mg_{37}Al_{26}Zn_{37}$ alloys, based on both the diffraction

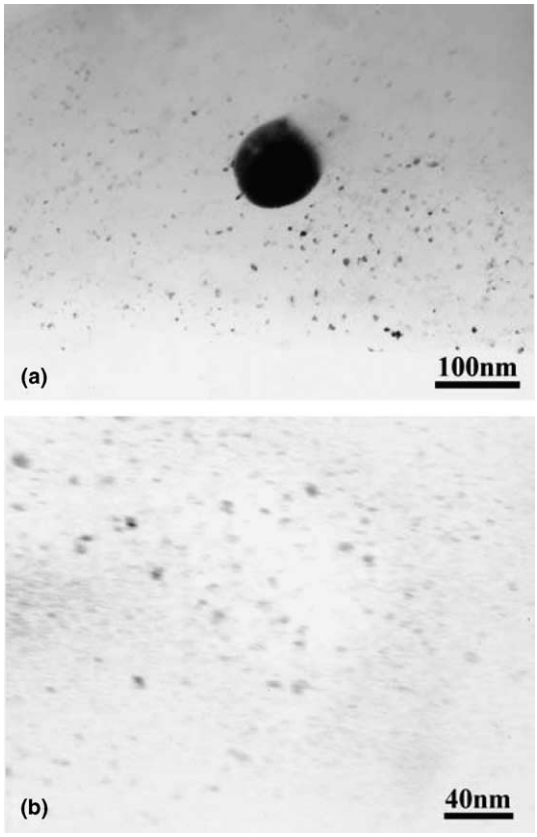

Fig. 12. (a) and (b) TEM micrographs showing the nano-sized $Mg_3Al_2Zn_3$ τ phase in the $Mg_{50}Al_{20}Zn_{30}$ alloy.

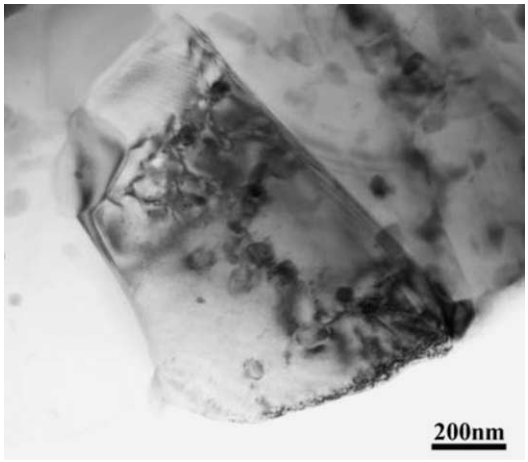

Fig. 13. TEM micrographs showing the fine Mg grains.

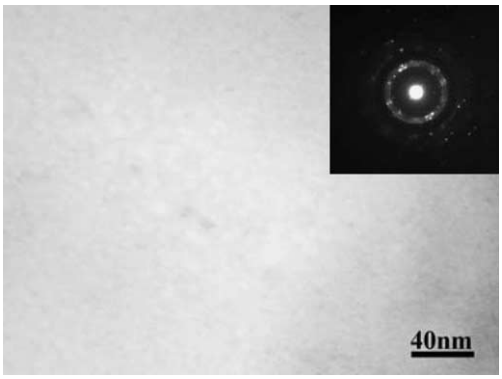

Fig. 14. TEM micrographs showing the incomplete amorphous region in the $Mg_{37.5}Al_{25}Zn_{37.5}$ alloy.

patterns and TEM/EDS measurements, has revealed the abundant $Mg_3Al_2Zn_3$ phase. In addition to the large particles (~3–10 μm) seen from both the SEM and TEM micrographs, there are many submicron- or nano-sized intermetallic phases, as shown in Fig. 12. The diffraction and EDS analyses suggest that these are mostly the $Mg_3Al_2Zn_3$, Mg_7Zn_3, and Al_2ZnMg phases. The grain sizes of the elemental Mg as seen in TEM micrographs are typically in the range of 0.05–1 μm (as shown in Fig. 13), which are also smaller than those seen in SEM. It means that the Mg phase observed in the SEM/BEI micrographs is actually composed of several submicron or nano-sized grains. This result signified the good grain refinement efficiency of FSP. Meanwhile, there are also some nano-scaled intermetallic phases with sizes near ~10–100 nm dispersed inside the Mg grain.

Based on the previous XRD patterns, the amorphous phase accounts is less than 5% in volume fraction. Hence, it is unusual to locate a massive amorphous volume under TEM. Only a few amorphous regions can be observed in the TEM micrographs. In Fig. 14, the observed region contains many fine nanocrystalline phases around 3–5 nm in size in the amorphous matrix.

4. Conclusion

1. The friction stir process was used to successfully fabricate bulk multi-element Mg base alloys with different fractions of AZ31 sheets, Al and Zn foils.
2. Multi-passes and high fractions of Al and Zn elements result in apparent grain refinement, proved by the broadening of diffraction peaks and from SEM results. After multi-passes, some intermetallic compound phases were generated.
3. The hardness of the multi-element Mg base alloy made by FSP reached the maximum value of nearly 400 H_v, especially in the $Mg_{37.5}Al_{25}Zn_{37.5}$ system or with liquid N_2 cooling, due to the generation of intermetallic compounds and grain refinement.

Acknowledgement

The authors gratefully acknowledge the sponsorship by the National Science Council of Taiwan, ROC, under the project no. NSC 93-2216-E-110-021.

References

[1] Thomas WM, Nicholas ED, Needham JC, Church MG, Templesmith P, Dawes CJ. Intl Patent No. PCT/GB92/02203.
[2] Mishra RS, Mahoney MW, McFadden SX, Mara NA, Mukherjee AK. Scripta Mater 2000;42:263.
[3] Ma ZY, Mishra RS, Mahoney MW. Acta Mater 2002;50:4419.
[4] Kwon YJ, Shigematsu I, Saito N. Scripta Mater 2003;49:785.
[5] Rhodes CG, Mahoney MW, Bingel WH, Spurling RA, Bampton CC. Scripta Mater 1997;36:69.
[6] Charit I, Mishra RS. Mater Sci Eng A 2003;359:250.
[7] Su JQ, Nelson TW, Sterling CJ. J Mater Res 2003;359:250.
[8] Chang CI, Lee CJ, Huang JC. Scripta Mater 2004;51:509.
[9] Berbon PB, Bingel WH, Mishra RS, Bampton CC, Mahoney MW. Scripta Mater 2001;44:61.
[10] Mishra RS, Ma ZY, Charit I. Mater Sci Eng 2003;A341:307.
[11] Lee CJ, Huang JC, Hsieh PL. Key Eng Mater, in press.
[12] Turnbull D, Fisher JC. J Chem Phys 1949;17:71.